Fermilab

6/5/92
TS-SSC 92-072

TO: Distribution

FROM: Jim Strait

SUBJECT: Summary of ASST magnet test data

Attached is a summary of test data from DCA311-319 which I have sent to Siegfried Wolff of DESY, who will be giving the summary talk on superconducting accelerator magnets at the XVth International Conference on High Energy Accelerators in Hamburg next month. This represents more or less the contents of a paper which Jozef will present on quench and strain gauge results and one which I will present on magnetic field measurements. Of course, any assistance any of you wish to give in preparing these papers will be much appreciated.

Distribution:
R. Bossert
J. Carson
S. Delchamps
A. Devred
J. DiMarco
W. Koska
M. Kuchnir
J. Kuzminski
T. Jaffery
M.J. Lamm
P.O. Mazur
D. Orris
J. Ozelis
E.G. Pewitt
J. Tompkins
M. Wake
Y. Yu
H. Zheng

Fermilab

6/5/92

To: Siegfried Wolff

From: Jim Strait

Subject: SSC Magnet Data

Attached are some SSC magnet test data from Fermilab. This note covers data to be presented at HEACC92 in a paper by Jozef Kuzminski on quench and strain gauge results and by me on magnetic field measurements. I am sorry that I did not get this to you by the 31 May deadline set by the conference organizers and hope that it is not too late for you to be able to use some of this material in your paper. Enclosed also are copies of several papers we presented at the International Industrial Symposium on the Super Collider in New Orleans in March.

MAGNET DESIGN

Figure 1 is a cross-section of the Fermilab design of the SSC collider dipole. The collars, made from 21-6-9 stainless steel, are 17 mm wide and have an outer radius of 67.82 mm. They serve to position the conductors as specified by the magnetic design and to provide restraint against conductor motion under excitation. As in the 40 mm dipoles the upper and lower collars are locked together by tapered keys and left-right pairs of collars are spot welded to give greater horizontal stiffness. The collars are sufficiently stiff by themselves to limit deflections to <0.1-0.2 mm under excitation. The collars do not use pole shims, and prestress is controlled by controlling the molded coil size. The cable is insulated with a the conventional Kapton plus fiberglass-epoxy tape.

The yoke has inner and outer radii of 67.81 mm and 165.05 mm given by the magnetic design. It contains various features for the bus work, helium flow and for mechanical assembly. The square holes at the mid-plane are of a size chosen to compensate for the effects of iron saturation on the harmonics after all the other feature sizes and locations were determined. The yoke is also used as a mechanical element to provide additional support to the collars to limit deflections under the Lorentz force. The collars are designed to have a small interference (0.08 mm on the radius) with the yoke near the horizontal mid- plane at the operating temperature of 4.35 K. The 4.95 mm thick, 340 mm O.D. 304LN stainless steel shell serves as a helium containment vessel and as a structure to clamp the two halves of the vertically split yoke together about the collared coil. The shell is made of two half-cylinders which are welded at the vertical parting plane of the yoke. The weld shrinkage pretensions the shell in the azimuthal direction to 200-250 MPa at 293 K. Due to the larger thermal contraction of the shell than the yoke the pretension grows to 350-400 MPa with cooldown and provides adequate clamping to restrain the Lorentz force up to fields well above the design operating point. With the collars supported by the yoke the coil deflections under excitation are <0.02 mm.

The coil ends have current blocks that match those of the 2-dimensional cross-section. The current blocks are defined by machined G10 spacers which incorporate internal supports under some of the cables. A "developable-surface, grouped" end design is used: the central cable of each current block follows a developable surface path which eliminates any "hard-way" bends, and the remaining cables are layed directly on each other with no spaces between them. No additional turn-to-turn insulation is used. The relative lengths of the current blocks are adjusted to minimize the integrated harmonics through the end.

The inner-outer coil splice is made outside the coil at the lead end. The coil ends and the splice are clamped by a collet clamp consisting of a 4-piece G10 insulator with a tapered outer surface and an aluminum cylinder with a tapered inner surface. An aluminum end cap is welded over the out-board end of the collet clamp. The upper-lower coil splice is enclosed under the lead end cap. A 38 mm thick end plate is welded to the end of the cold mass shell. The end coil is preloaded axially against the end plate with four set screws at each end to provide axial restraint under excitation.

INSTRUMENTATION

The magnets are instrumented with 53 voltage taps, concentrated on the inner coil turns nearest the pole, and strain gauge load cells to measure coil azimuthal stress and axial force at one end. The azimuthal coil stress gauges are placed at two locations, where the average coil size is largest and smallest. Most of the coil size variation is systematic and the essentially the same pattern is observed in both inner and outer coils, therefore the small and large points are the same for the inner and outer coils.

MAGNET SERIES

The data shown here are from the first 9 of a series of 13 magnets that are being built at Fermilab. The first (DCA311) was built by Fermilab technicians. The second (DCA312) was the "technology transfer magnet" and was built jointly by Fermilab and General Dynamics technicians. The next 7 (DCA313-319) were built by General Dynamics. However, Fermilab personnel still operated the major tooling, provided the weldors, performed assembly of items that would not be part of production magnets (e.g. voltage taps), and oversaw the QA program. Five of these 7 GD-built magnets are being installed in the Accelerator Systems String Test (ASST) which is currently being set up at the SSCL in Texas.

The last four magnets (DCA320-323) are currently being built by Fermilab technicians and use an epoxy coated Kapton insulation system similar but not identical to that used on the low-beta quadrupole. Two different variants are being used with insulation and adhesive from two different vendors each. Assembly of this series is well along and we may have the first test results just in time for the conference.

HARMONICS DATA

Field harmonics are measured using the BNL "Mole" on each magnet at room temperature before and after the yoke is assembled, and at 4.35 K. Attached is a table of the mean and RMS values of the harmonics averaged over the length of the magnet at 2 T (2 kA). (You of course recall that on this side of the Atlantic b2 is the sextupole, etc. The units are 10**-4 of the dipole field at

1 cm.) No correction have been made to the allowed multipoles for the effects of persistent currents. (At 2 T on the up-ramp the persistent current components of b2 and b4 are approximately -0.35 and +0.02 respectively.) The data are taken at a time sufficiently long after the DC current level has been established that any time dependent effects are believed to have decayed to a negligible level. Based on uncertainties in the centering corrections (until an improved support was installed for the "warm finger" for the last 3 magnets the probe was significantly off center) and discrepancies between measurements made with the probe inserted from opposite ends of the magnet, we are not confident about the measurements of the high-order unallowed harmonics, and therefore we do not present them here.

Figures 2-4 graphically present the mean values of the harmonics for the nine magnets. The data point is the mean value, and the error bar is the RMS divided by the square-root of 9 and represents the uncertainty in the estimate of the mean of the underlying distribution, assuming that these nine magnets are representative of the full production. In Figures 2 and 3 the values are plotted directly; two different vertical scales are used to allow both the low and high order harmonics to be seen. The horizontal dashes indicated the specified limits on the mean over the whole production. Figure 4 is a plot of the mean divided by the specification limit. Figure 5 is a plot of the one-sided 95% confidence bounds on the RMS of the underlying distribution, again assuming that these 9 magnets are representative of a full production run.

All of the allowed harmonics are systematically shifted from zero by amounts larger than the specifications. If this magnet design were to be used for the SSC small adjustments would have to be made in the cross-section to set these harmonics to zero. The quoted RMS for the allowed harmonics is computed about the mean value, since the mean is clearly non-zero. It is conjectured that much or all of the difference between the design and measured allowed harmonics comes from the greater compression of the coil near the mid-plane which may be induced by frictional effects in the molding or the collaring process. Calculations indicated that values comparable to those observed can be generated by plausible conductor displacements of this sort. Measurements on coil cross sections are being carried out at the SSCL which should allow us to determine if this conjecture is correct.

For the unallowed harmonics, we have insufficient data to show whether the true distribution has a non-zero mean. Therefore the RMS is computed about zero. The average of each of the unallowed harmonics, with the exception of the skew sextupole a2, is, within statistical uncertainty, consistent with zero. However the number of magnets is too few to project if a production series would have averges within the specifications, particularly for the normal and skew quadrupole moments b1 and a1. The mean value of the skew sextupole is a little more than 2 standard deviations from zero. This results from a systematic molding of the coils with one side 8-10 microns bigger than the other. This results in a left-right asymmetric mid-plane shift, which generates all the ~~odd~~ even skew multipoles. (The effect on poles higher than a2 is too small to observe.) Although this is systematic in our coils, we presume that in a larger production run using several sets of tooling, such an effect would average to zero. Even with this systematic effect, the 95% confidence limit on the RMS about zero is less than the specification. (See Figure 5.)

While there is a systematic 8-10 micron left-right assymmetric mid-plane shift, there is no systematic left-right symmetric mid-plane shift. Based on coil size measurements the RMS mid-plane shift, which generates principally the skew quadrupole moment a1, is 10 microns, with the largest shift being less than 25 microns. Figure 6 is a plot of the measured skew quadrupole versus that computed from coil size differences. The correlation is reasonable. Figure 7 shows the measured skew sextupole versus that computed from the left-right coil size differences. The correlation is not as good as that for a1, but measurement and calculation agree on the sign in all but one case.

It is striking that for all measured harmonics the RMS widths are considerably smaller than the allowed values. Perhaps most notable is the skew quadrupole term (a1). No effort has been made to match upper and lower coils by size, except that in most cases the coils are matched by conductor vendor and often by reel number. The RMS specification of 1.25 units is based not on what is desired from accelerator physics considerations, but on what was estimated to be achievable based on extrapolation from HERA experience. The accelerator physics requirement is comparable to that for the normal quadrupole (b1), or 0.5 units. In this series of magnets we have met the tighter specification. Assuming that the production magnets would come from the same distribution, then the RMS a1 for magnets made the same as ours is < 0.67 at a 95% confidence level.

Figure 8 is a plot of sextupole (b2) versus current in a 1.5 m model magnet. The effect of the mid-plane cutout, whose purpose is to limit the iron saturation effect on b2, is visible. Just above 4 kA b2 begins to drop, as the iron at the inner radius near the pole begins to saturate. Above 5 kA (5 T), it begins to rise as the mid-plane iron saturates in the presence of the cutout. Starting between 6.5 and 7 kA, b2 begins to drop again as the pole saturation becomes stronger. Data from a typical long magnet are shown in Figure 9. The iron saturation pattern here is considerably different, with a much greater increase above 5 kA. This is believed to result from the presence of the soft iron cryostat vacuum vessel, which reduces the effect of mid-plane saturation. A few tenths of a unit of iron saturation skew quadrupole also results from the fact that the magnet is vertically off-center in the cryostat. The new GD design incorporates an up-down asymmetry in some yoke features to try to cancel the latter effect.

FIELD STRENGTH DATA

The field strength is measured near 2 T using an NMR probe. The measured ratio B/I, averaged over the 9 magnets, is 1.0452, with an RMS variation magnet-to-magnet of 2 parts in 10**4. (See the table of harmonics) This is very close to the value of 1.0451 computed by Ramesh Gupta of BNL for this design. The magnetic length is measured by integrating the NMR measurements in the body of the magnet and Hall probe measurements through the end fields. The RMS variation in the magnetic length is also 2 parts in 10**4. Given the measured magnetic length, these magnet must be run at a field of 6.733 T at 6644 A to achieve the required field integral of 100.09 Tm.

STRAIN GAUGE DATA

Figure 10 is a plot of coil stress versus I**2 for a typical magnet. (This is "typical" in the sense that it has been randomly selected.) Each curve is the average of four gauges in the inner or outer coil quadrants at each of the large and small spots on the coils. The stress (I apologize for the folk units ... 1 kpsi = 6.9 MPa) is essentially linear up to the highest current measured (just over 8 kA, or about 8T) and that the prestress is still positive even at this high current (22% in current or almost 50% in force above the operating current of 6.6 kA, or 44 kA**2).

Figure 11 is a plot of the force between the coil end and the end plate as a function of I**2 for the same run. (1000 pounds = 454 kg = 4444 Newtons.) The dependence on I**2 is linear and the force change to 8 kA, 7300 pounds = 33 kN, is less than one quarter of the total axial Lorentz force. That is, only a small fraction is carried by the coil end in compression and the majority of the force is carried by the coil in tension and then via coil-collar-yoke-shell friction to the outer shell.

QUENCH DATA

Figure 12 is a plot of the initial quenches of the 9 magnets. Four of the magnets, DCA313, 314, 316 and 317, had training quenches below the operating current. In three of the four cases (DCA313, 314 and 317) the quenches were in the indentical location within the few cm resolution of the position determination from the voltage taps. This location is at or near the boundary between the collet end clamp and the collared part of the coil. It is believed that these result from a minor design flaw, in which the pole end key, which was originally designed as a single piece, was made into two pieces to aid assembly. There is no way, however, to ensure that the small piece, which is adjacent to the quench location, is properly seated during assembly. We believe that the quenches result as this piece moves into place. This modification was implemented after the first 2 magnets. A series of 7 1.5 m models, all of which were built with the original 1 piece key, show no training. The fourth low quench (DCA316) is in an uninstrumented portion of the coil, so neither its precise location nor its cause is known.

Several low quenches result from operation at higher than the SSC specified ramp rate of 4 A/sec and from the surprisingly large ramp rate dependence of the quench current in most of these magnets. (See below.) The quenches that result from ramp rate heating are labeled with their ramp rates. For all other quenches the ramp rate is 4 A/sec or less. Other fluctuations in the plateau quench currents observed for all of the magnets results from fluctuations in the test temperature.

On the second cooldown no magnets had any low quenches. Low temperature runs were made on the second cooldown, first at 3.8 K and then at 3.5 K. Several of the magnets have one or two training quenches at one temperature or the other. DCA314 began to show progressively worse quench performance at 3.5 K after reaching 8.4 kA (8.3 T). It returned, however, to its previous plateau at 4.35 K. Schedule pressures prevented us from attempting to understand this behavior. (Note, open circles represent quenches which originated in the outer coil.) Differences between the ratio of plateau currents at the two temperatures results from the different Jc vs. T dependence of cable from different vendors.

Figure 13 is a plot of the quench current versus ramp rate for the 9 magnets. There is considerable magnet-to-magnet variation both in the degree of ramp-rate dependence and in the shape of the curve. The ramp rate dependence is generally quite dramatic; the worst magnet (DCA312) quenches at only 2 kA at 200 A/sec. Of course, since the collider operates at 4 A/sec, this is not really a problem. However, the high energy booster is to use essentially the same magnet, and there such a ramp rate dependence cannot be tolerated.

The general shape of the curve (concave up or down) correlates with conductor vendor. A solid line in Fig. 13 indicates cable from IGC, a dotted line Oxford, and the dot-dashed line Supercon. However, among the magnets made from wire from a single vendor there is wide variation in the ramp rate sensitivity. This suggests that there is some variable in the manufacturing process (somewhere from the wire manufacturing through the final magnet assembly) which is not adequately controlled. Presumably this si something that affects the strand-to-strand resistance within the cable.

AC LOSS DATA

To study this issue further we have measured the energy loss per cycle as a function of ramp rate for 6 of the 9 magnets. (Schedule pressures prevented the measurement being made on two others and there was a problem with the readout system during measurement of another.) The data, taken on 500-5000-500 A cycles, are shown in Figure 14. Shown also is the average of measurements of four 1.5 m model magnets, multiplied by 10, which is roughly the ratio of magnetic lengths. There is considerable variation among these magnets in the eddy current (dI/dt) term. The apparent spread in hysteresis loss is a little larger than what we think is the experimental uncertainty, but we do not understand the cause of this. The magnets with the weakest and strongest quench dependence on ramp rate also have respectively the smallest and largest eddy current losses. This is quantified in Figure 15, where the slope of the ramp rate dependence of the quench current (fit for 50 A/sec and above) is plotted versus the eddy current loss. The dashed line is a fit to the long magnet data which is forced to go through the origin and it is meant only to guide the eye. The good correlation between the ramp rate dependence of the quench current and the eddy current losses suggests that the variability in the ramp rate dependence results from variations in the energy loss rather than from differences in the cooling efficiency.

Field Harmonics at 2 T
of
Nine Fermilab/GD-Built SSC Dipole Magnets

Uncorrected for superconductor magnetization

	Mean	SSC Spec	RMS	SSC Spec
Allowed Harmonics				
b_2	1.5	0.8	0.39	1.15
b_4	0.30	0.08	0.03	0.22
b_6	-0.043	0.013	0.004	0.018
b_8	0.051	0.010	0.0012	0.0075
Unallowed Harmonics				
b_1	0.03	0.04	0.178	0.5
b_3	0.001	0.026	0.028	0.16
b_5	0.001	0.005	0.003	0.017
a_1	0.03	0.04	0.39	1.25
a_2	0.114	0.032	0.16	0.35
a_3	-0.002	0.026	0.06	0.32
a_4	0.006	0.010	0.02	0.05
a_5	0.002	0.005	0.01	0.05
B/I	1.0452		0.0002	
L_{mag}	14.865		0.003	

SSC Collider Dipole Magnet
(Fermilab Design)

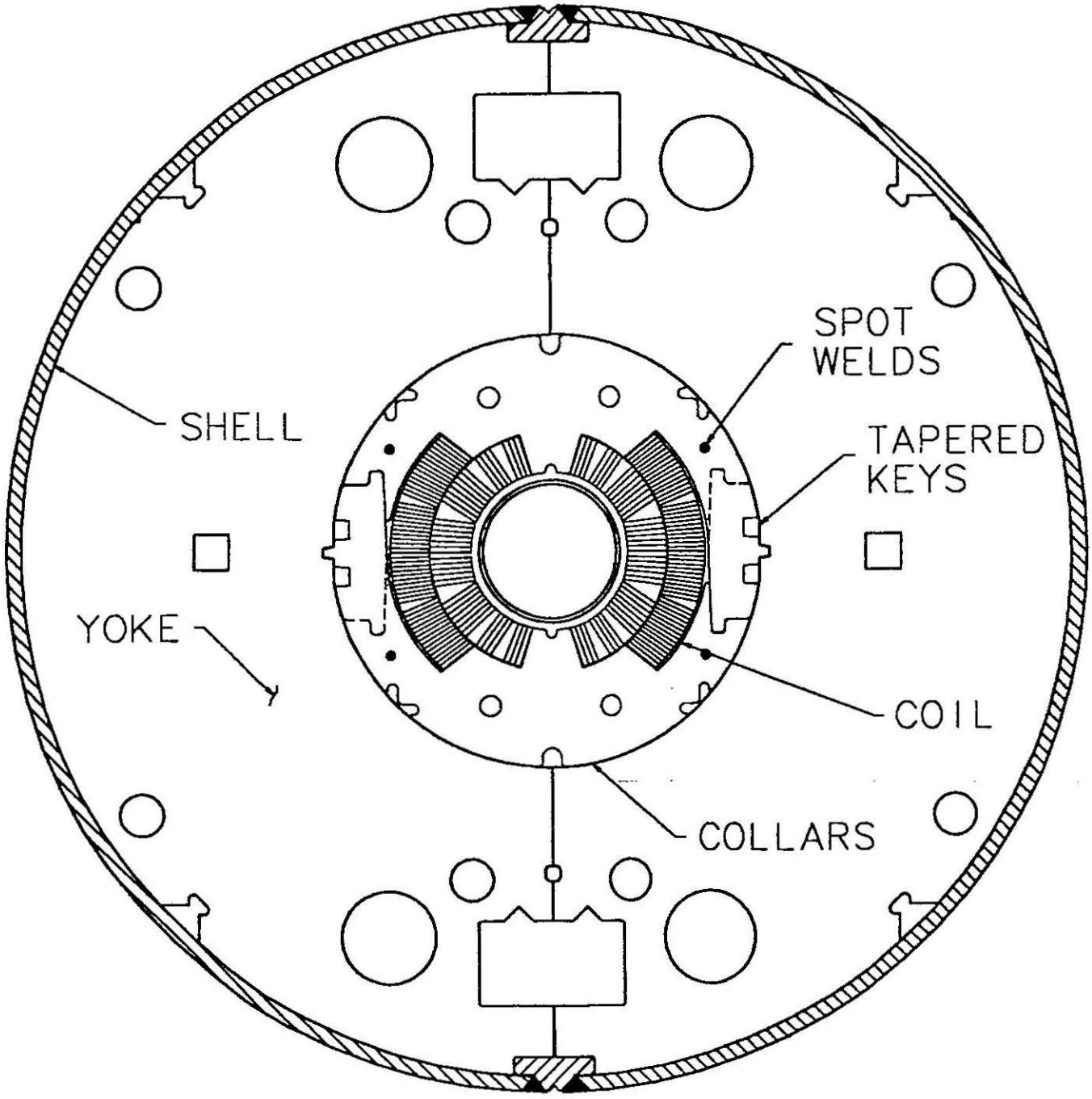

Figure 1
SSC Collider Dipole Magnet Cross Section

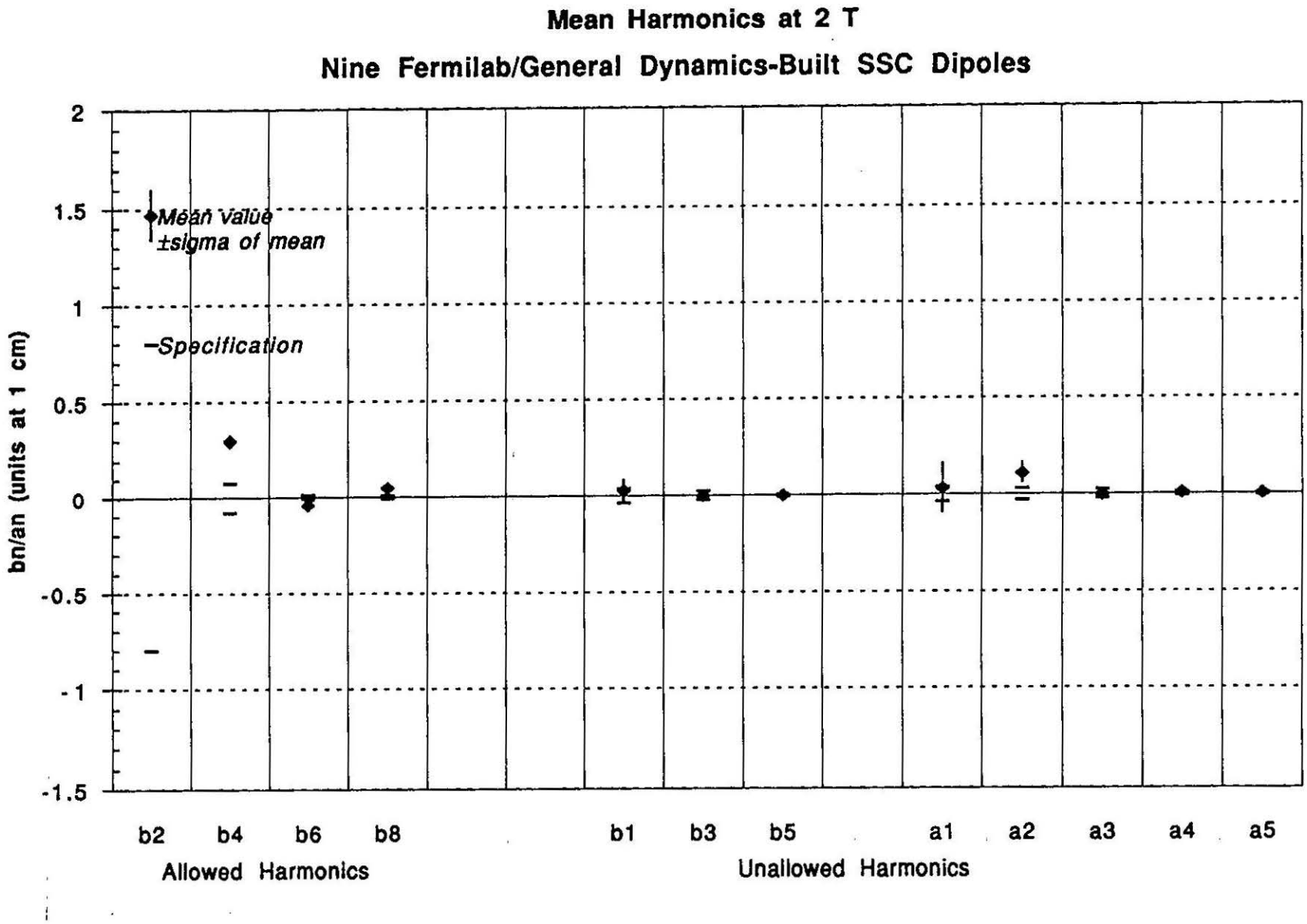
Mean Harmonics at 2 T
Nine Fermilab/General Dynamics-Built SSC Dipoles
bn/an (units at 1 cm)
2
1.5
1
0.5
0
-0.5
-1
-1.5
Mean value
±sigma of mean
Specification
b2
b4
b6
b8
b1
b3
b5
a1
a2
a3
a4
a5
Allowed Harmonics
Unallowed Harmonics

Figure 2

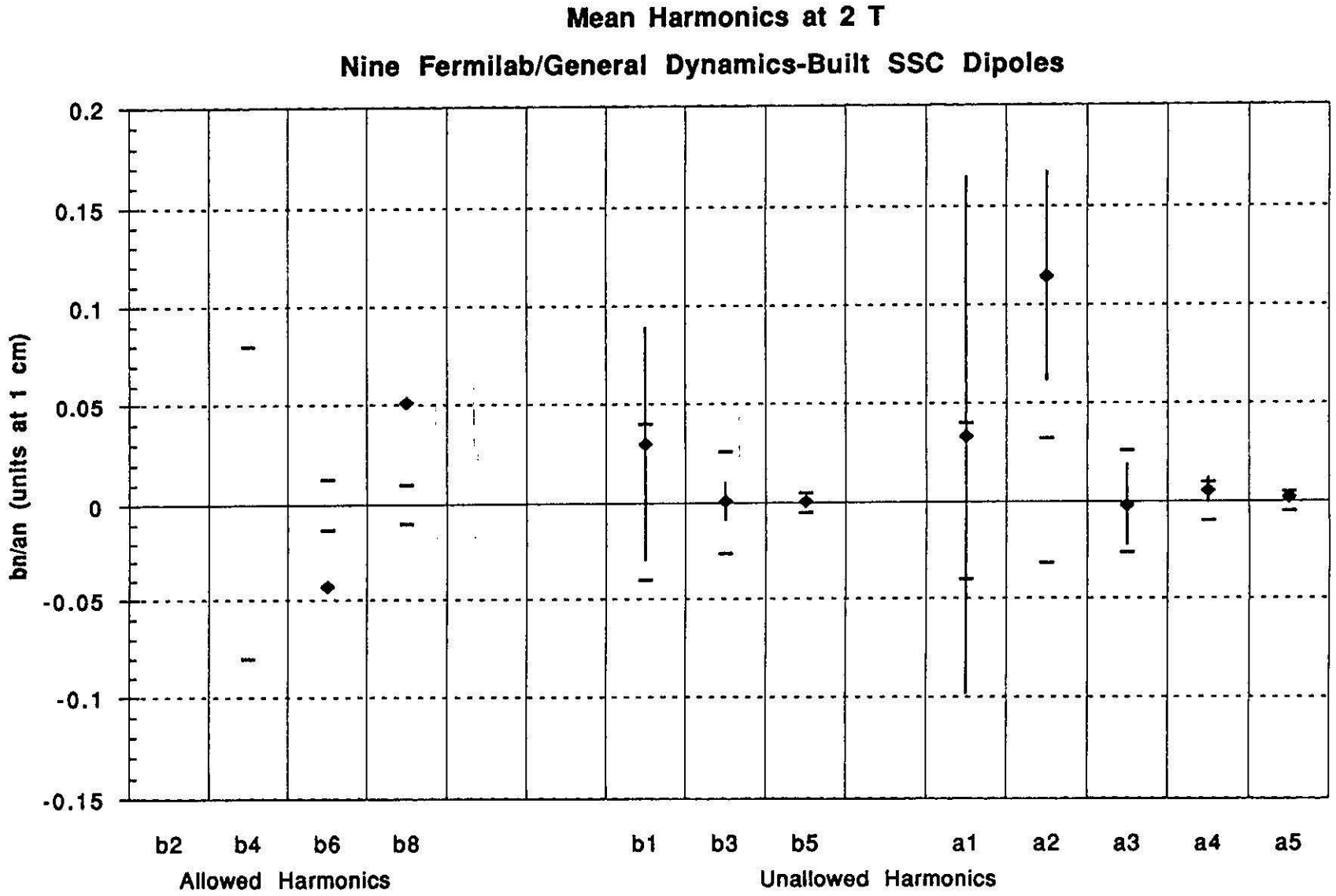
Mean Harmonics at 2 T
Nine Fermilab/General Dynamics-Built SSC Dipoles
bn/an (units at 1 cm)
0.2
0.15
0.1
0.05
0
-0.05
-0.1
-0.15
b2
b4
b6
b8
b1
b3
b5
a1
a2
a3
a4
a5
Allowed Harmonics
Unallowed Harmonics

Figure 3

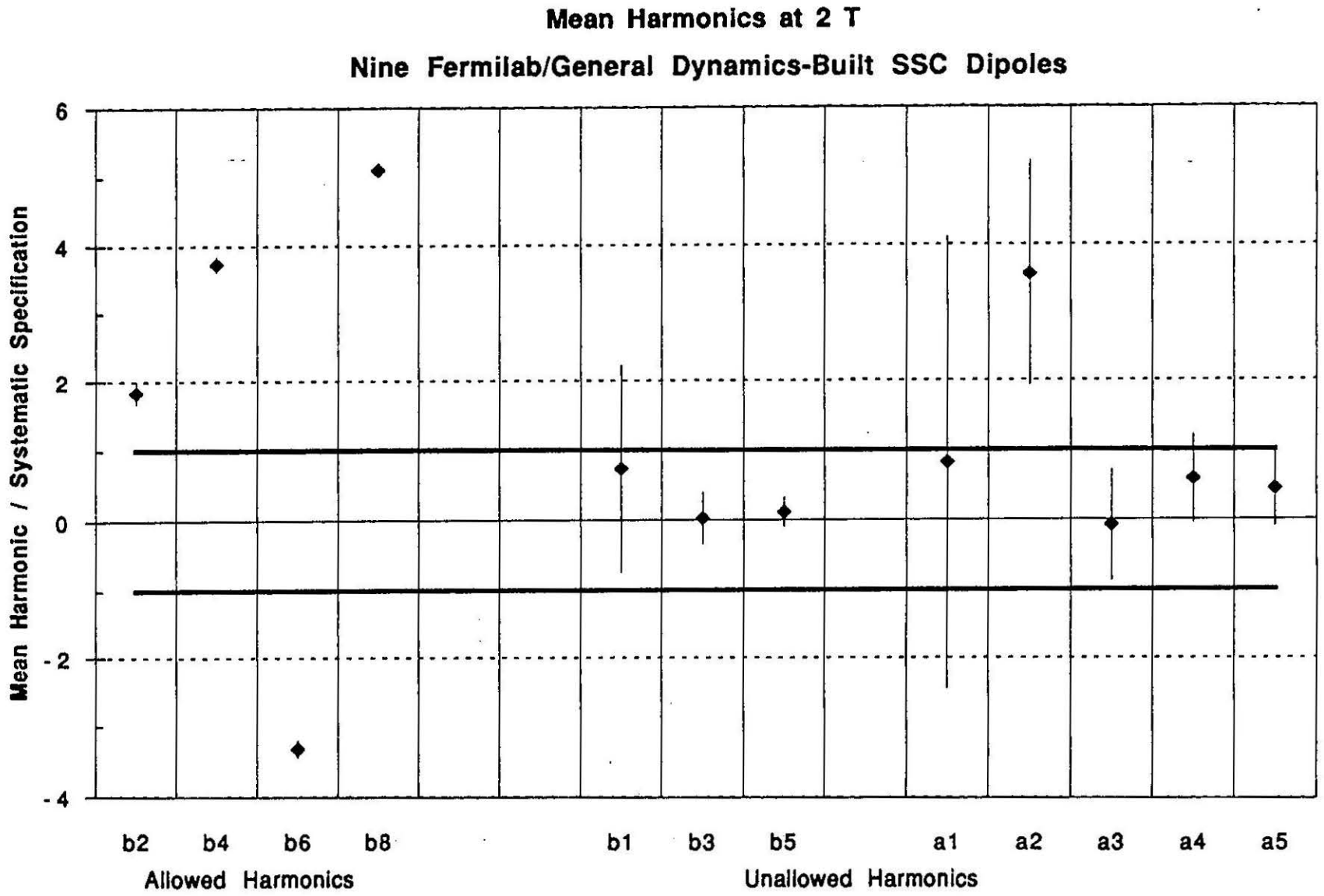
Mean Harmonics at 2 T
Nine Fermilab/General Dynamics-Built SSC Dipoles
Mean Harmonic / Systematic Specification
6
4
2
0
-2
-4
b2
b4
b6
b8
b1
b3
b5
a1
a2
a3
a4
a5
Allowed Harmonics
Unallowed Harmonics

Figure 4

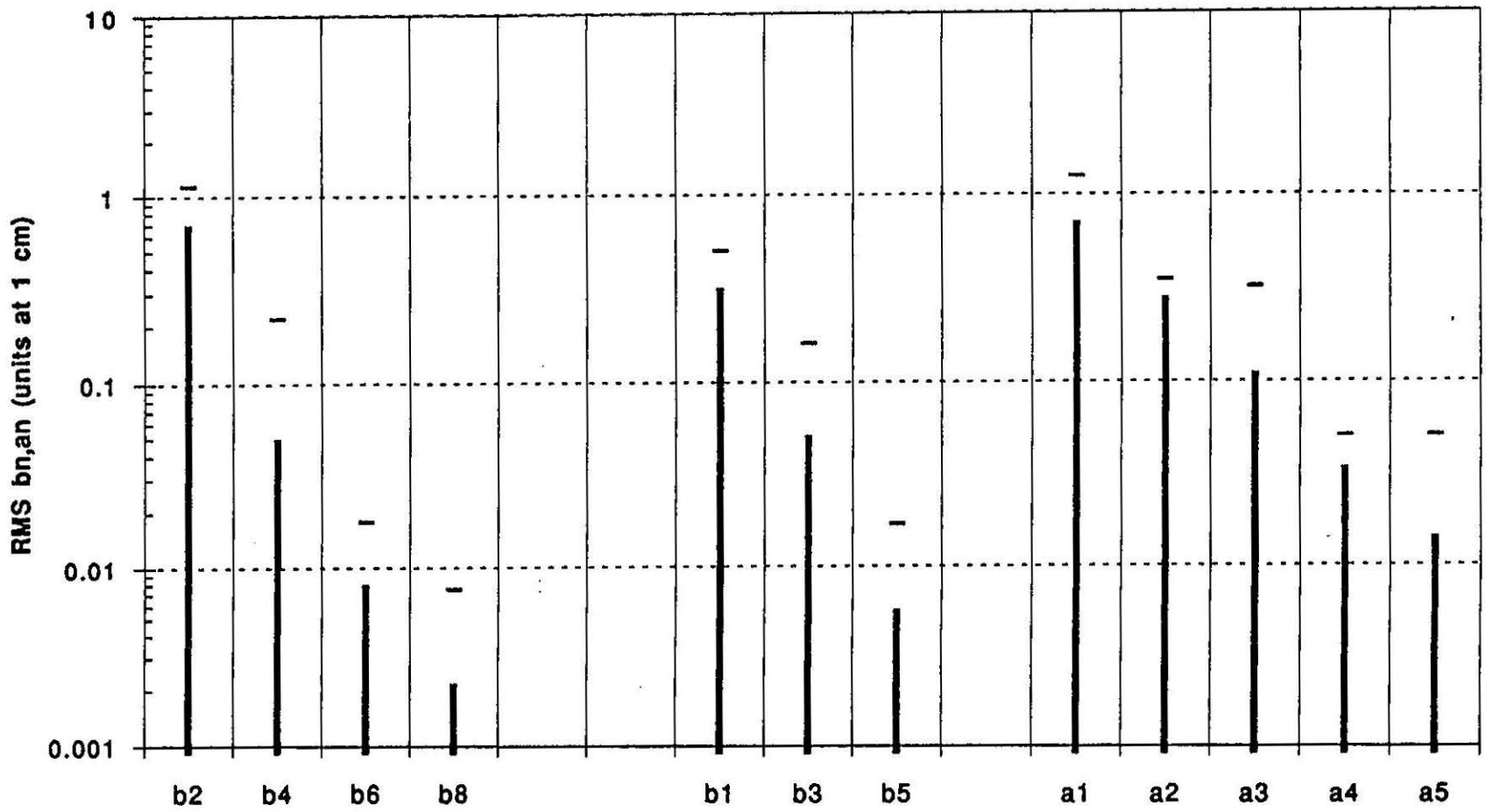
95% C.L. Upper Bounds on RMS Variations in Harmonics:
Nine Fermilab/General Dynamics-Built SSC Dipoles
RMS bn,an (units at 1 cm)
10
1
0.1
0.01
0.001
b2
b4
b6
b8
b1
b3
b5
a1
a2
a3
a4
a5

Figure 5

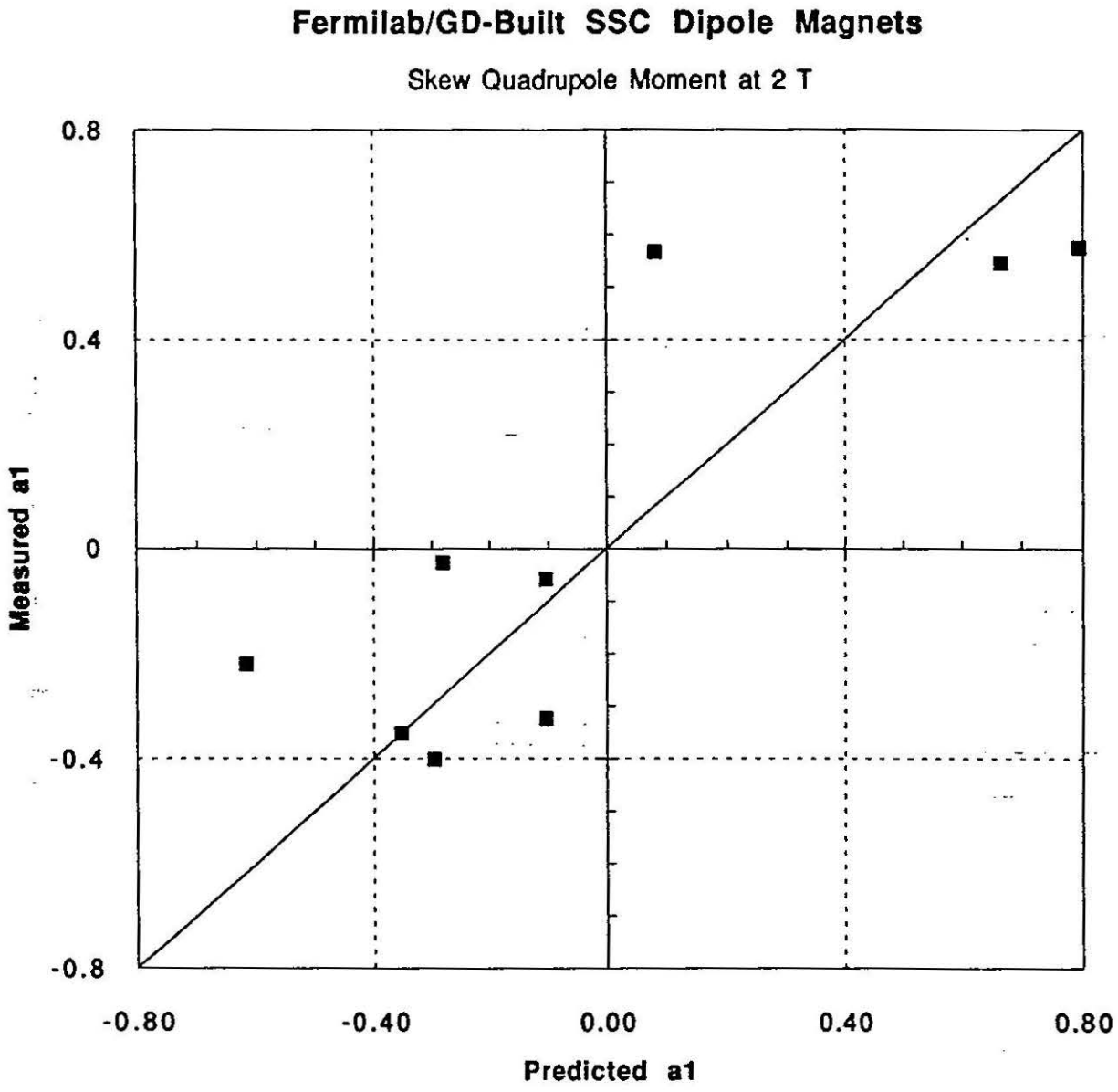
Fermilab/GD-Built SSC Dipole Magnets
Skew Quadrupole Moment at 2 T
0.8
0.4
0
-0.4
-0.8
Measured a1
-0.80
-0.40
0.00
0.40
0.80
Predicted a1

Figure 6

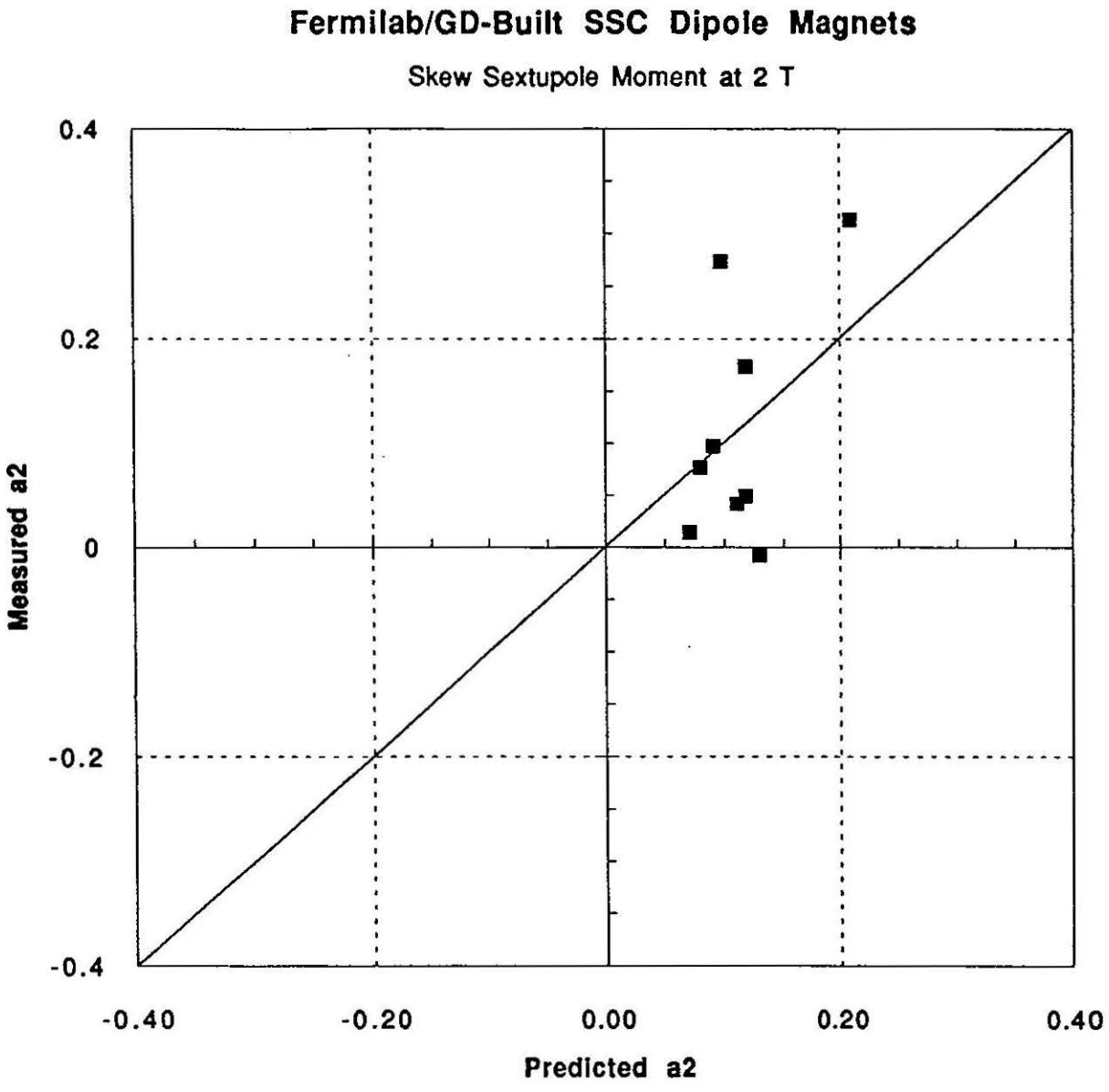
Fermilab/GD-Built SSC Dipole Magnets
Skew Sextupole Moment at 2 T
Measured a2
Predicted a2
0.4
0.2
0
-0.2
-0.4
-0.40
-0.20
0.00
0.20
0.40

Figure 7

Fermilab-built 1.5 Model SSC Dipole Magnet

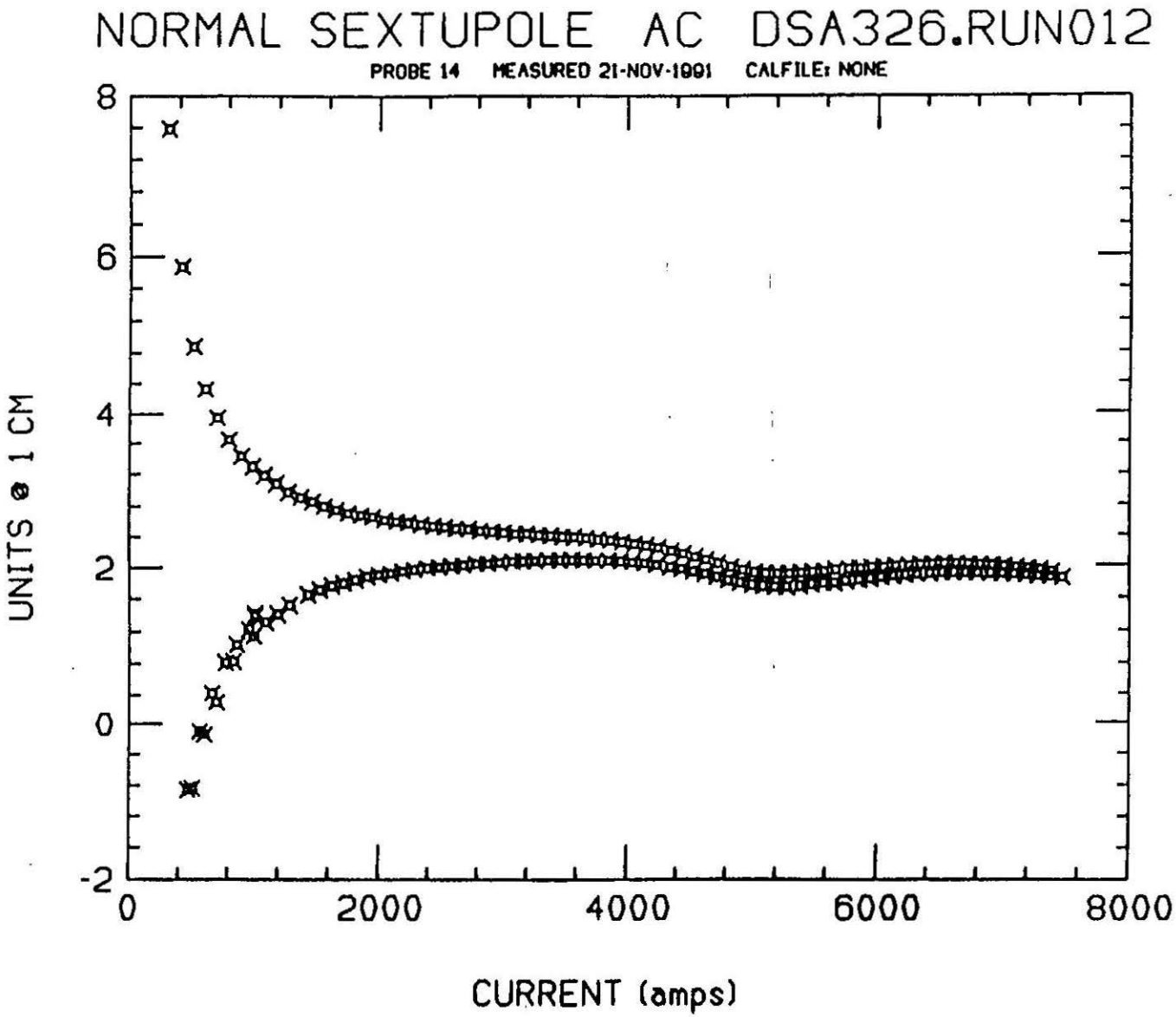

Figure 8

Fermilab/GD-built SSC Dipole Magnet

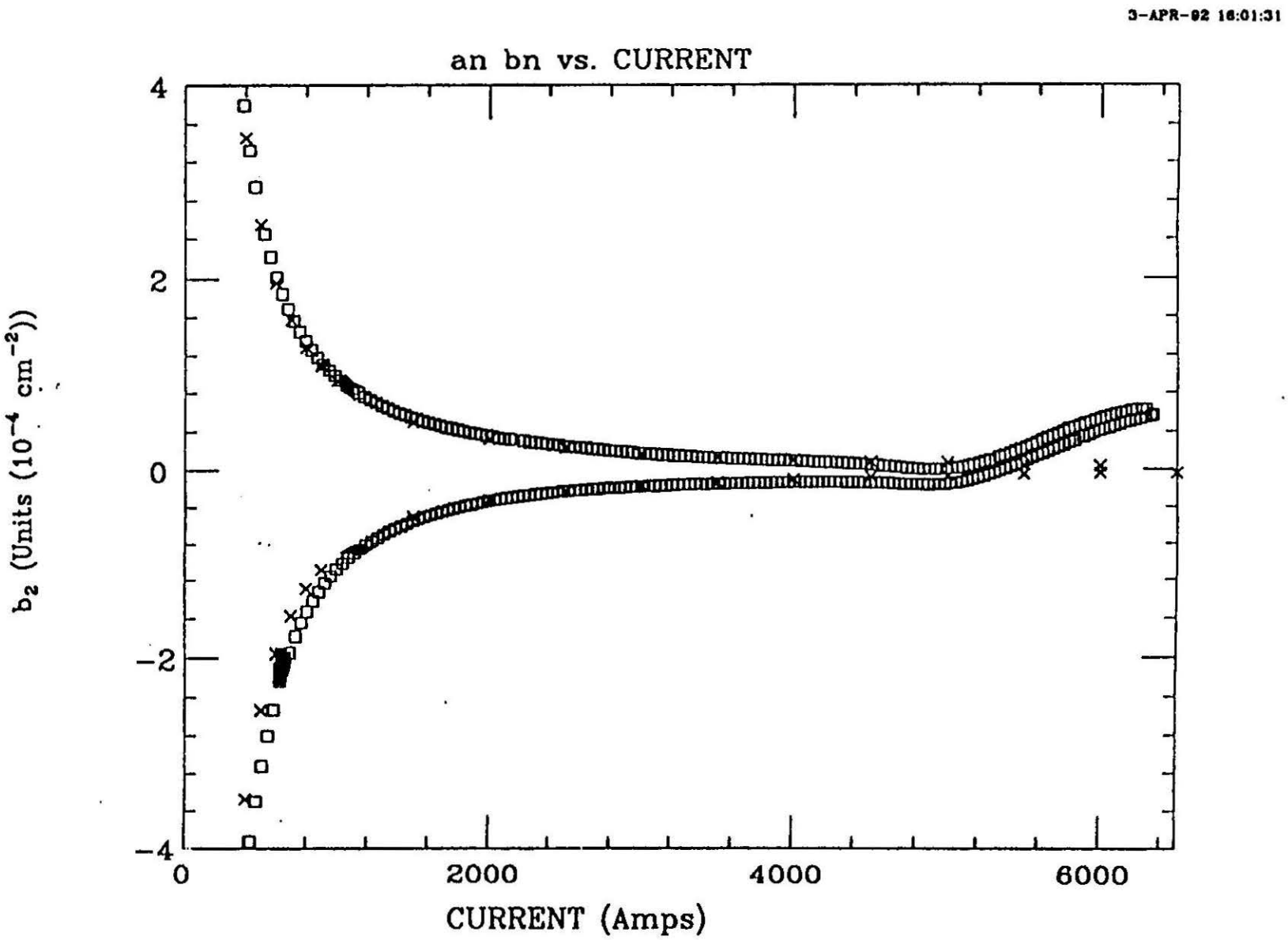

DCA317 518 10 Apr 1992 cold position (M) : 0.3560000
Jc(IU)=2811 A/mm^2 Jc(IL)=2912 A/mm^2
Jc(OU)=2968 A/mm^2 Jc(OL)=2968 A/mm^2

× Theoretical model
□ Measurement results

Figure 9

Fermilab/GD-built SSC Dipole Magnet

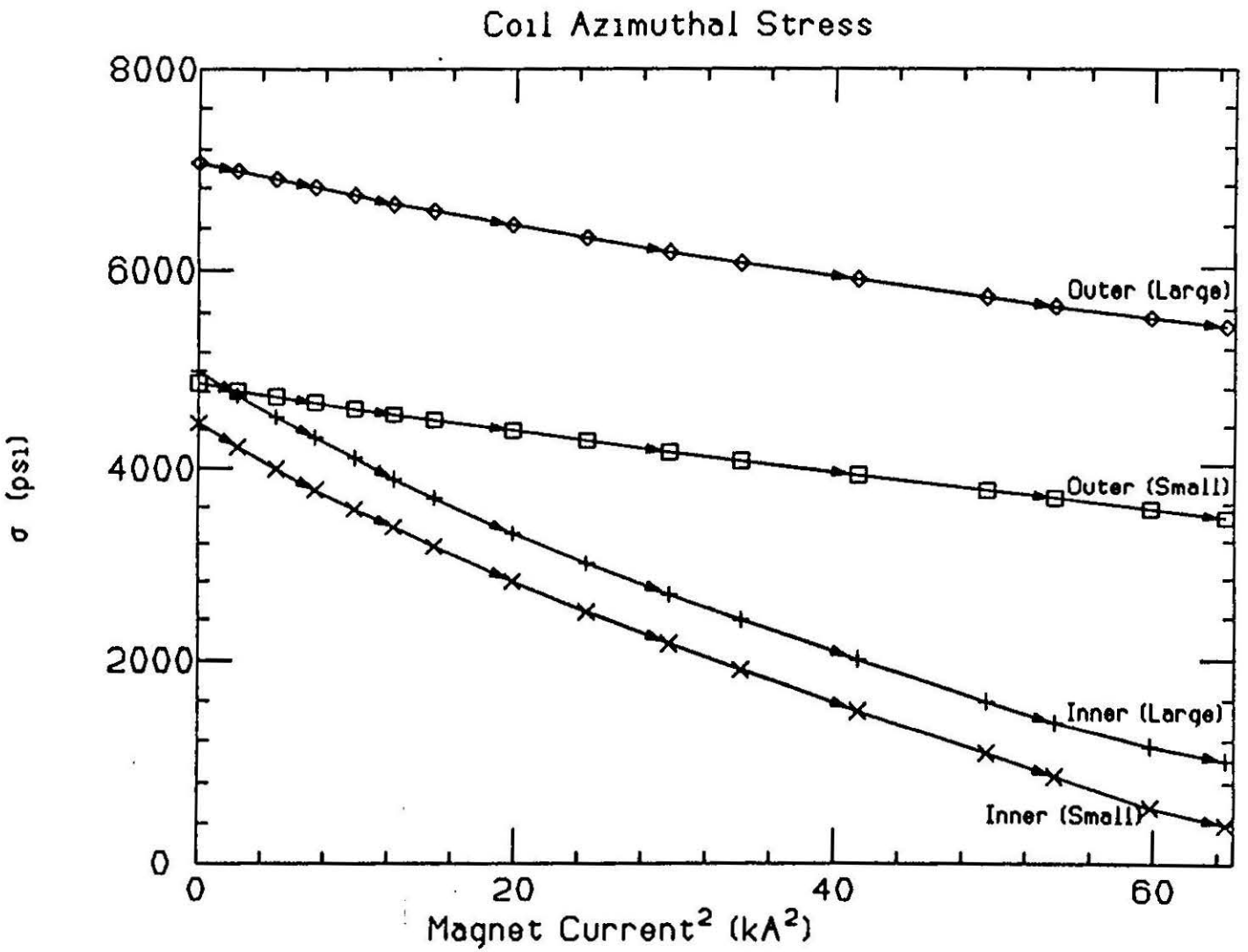

DCA314 File: DCA314.CA011 5-FEB-92 06:37:48 17-FEB-92 15:13:25

Figure 10

Fermilab/GD-built SSC Dipole Magnet

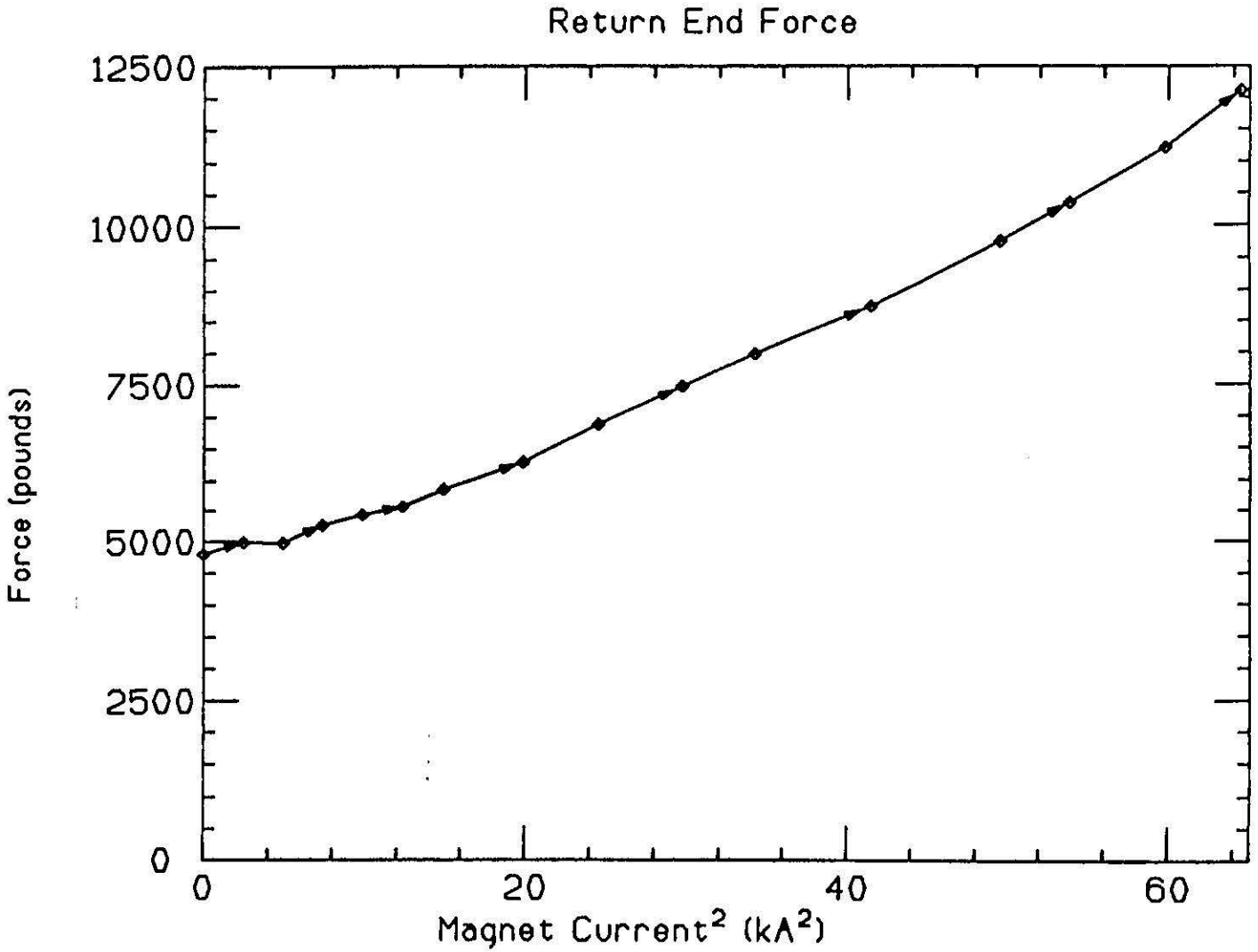

DCA314 File: DCA314.CA011 5-FEB-92 06:37:48 17-FEB-92 15:13:25

Figure 11

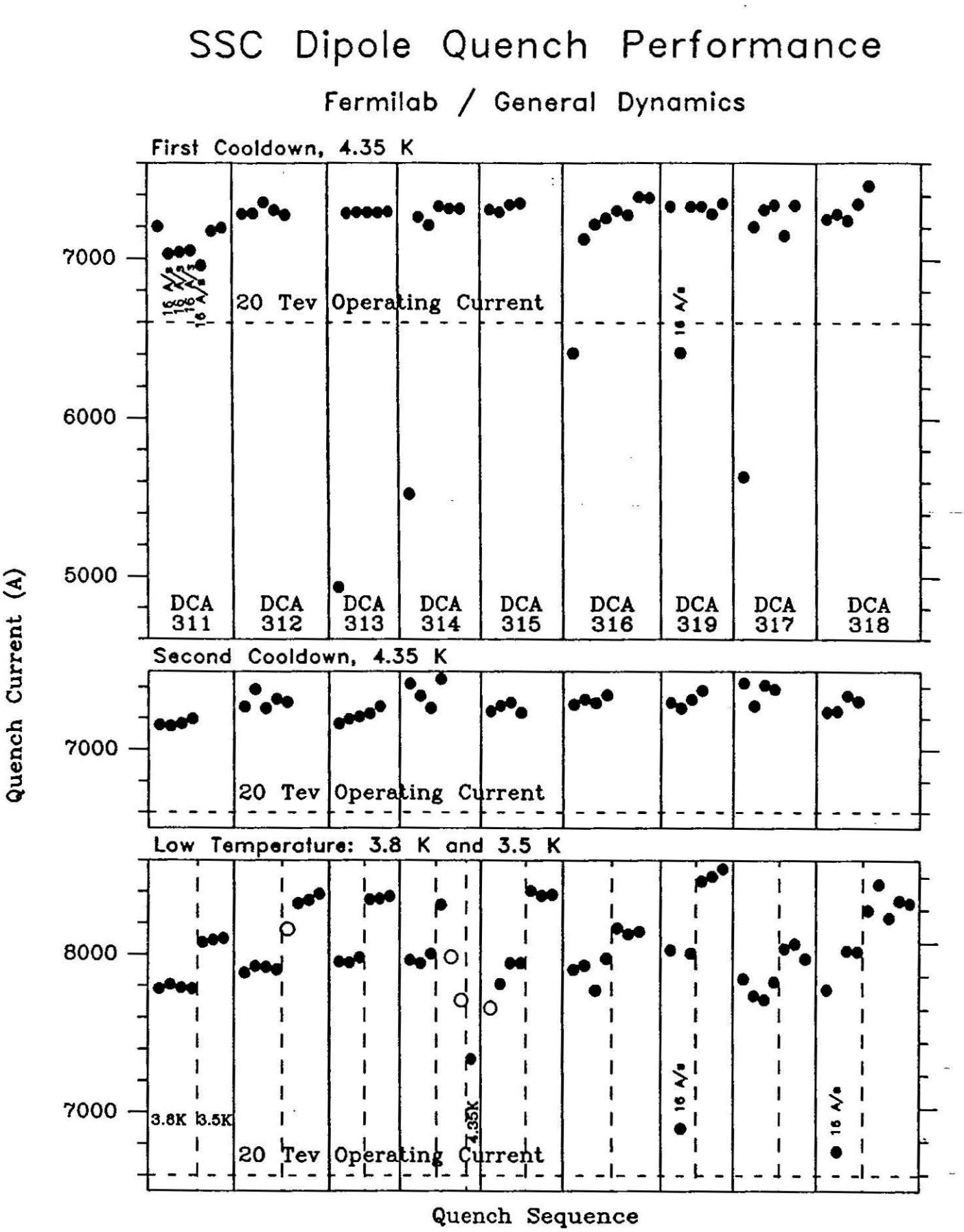
SSC Dipole Quench Performance
Fermilab / General Dynamics
First Cooldown, 4.35 K
20 Tev Operating Current
16 A/s
DCA 311
DCA 312
DCA 313
DCA 314
DCA 315
DCA 316
DCA 319
DCA 317
DCA 318
Second Cooldown, 4.35 K
20 Tev Operating Current
Low Temperature: 3.8 K and 3.5 K
3.8K
3.5K
4.35K
20 Tev Operating Current
16 A/s
Quench Current (A)
5000
6000
7000
8000
Quench Sequence

Figure 12

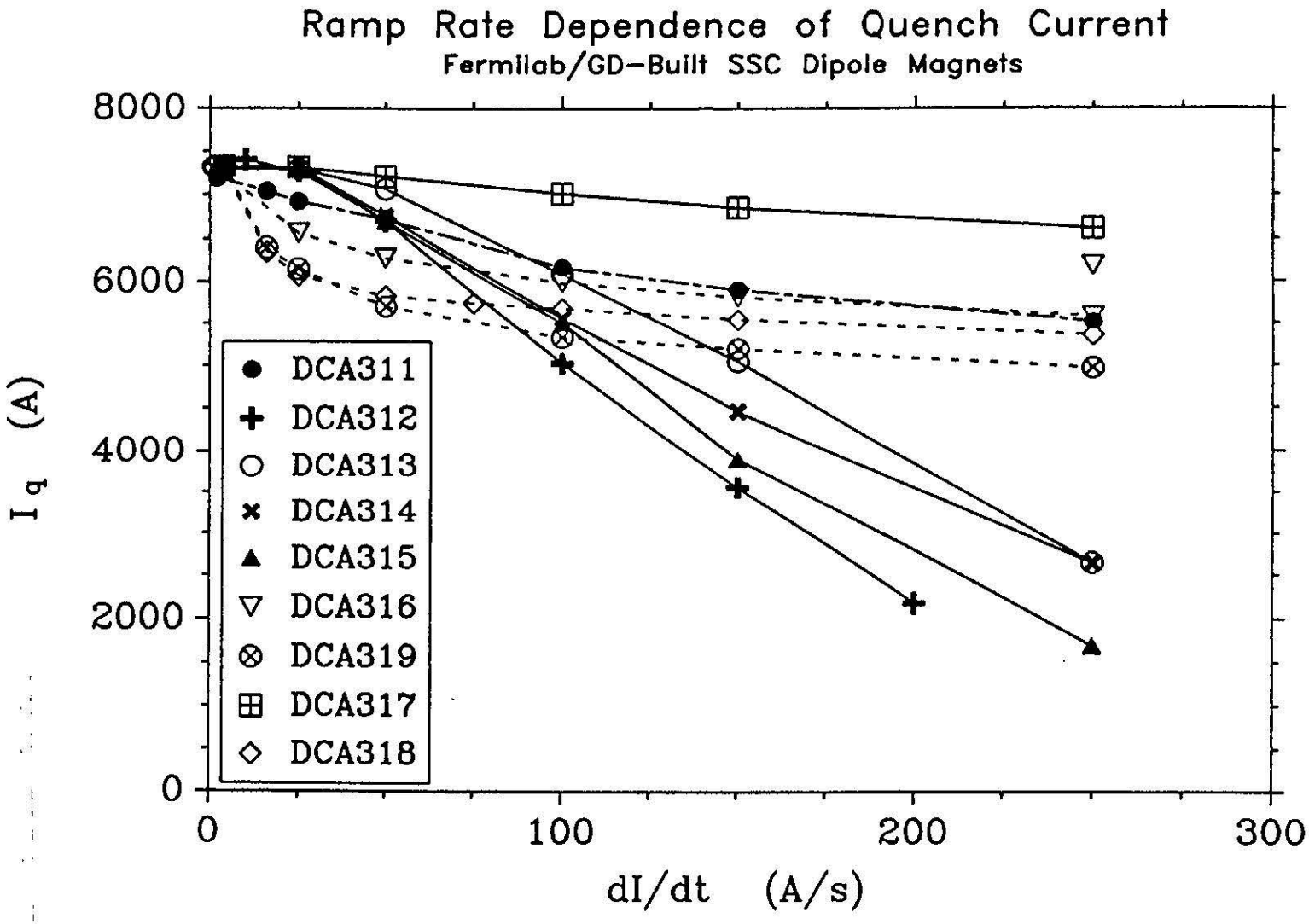
Ramp Rate Dependence of Quench Current
Fermilab/GD-Built SSC Dipole Magnets
8000
6000
4000
2000
0
I_q (A)
0
100
200
300
dI/dt (A/s)
DCA311
DCA312
DCA313
DCA314
DCA315
DCA316
DCA319
DCA317
DCA318

Figure 13

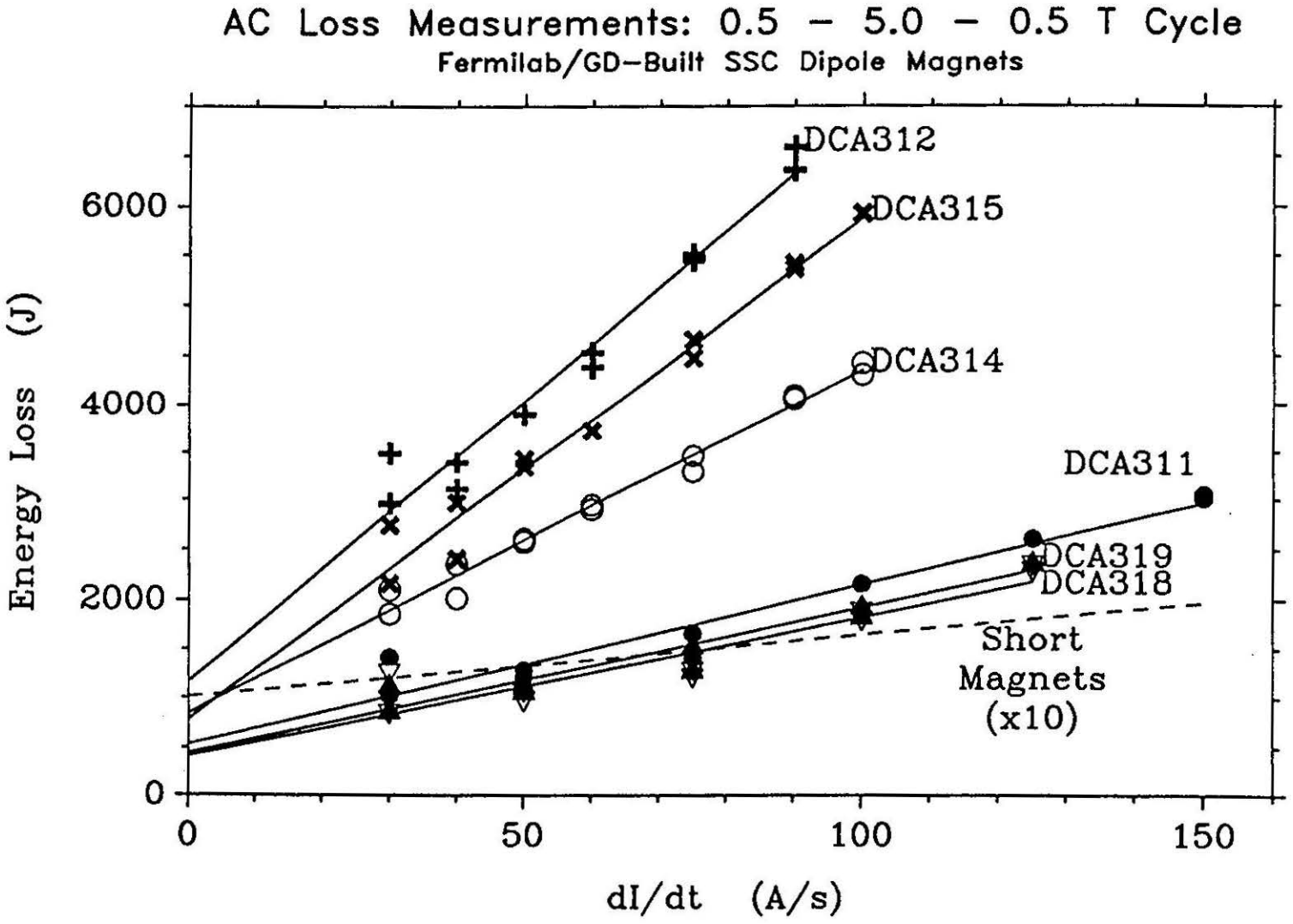
AC Loss Measurements: 0.5 – 5.0 – 0.5 T Cycle
Fermilab/GD–Built SSC Dipole Magnets
Energy Loss (J)
6000
4000
2000
0
0
50
100
150
dI/dt (A/s)
DCA312
DCA315
DCA314
DCA311
DCA319
DCA318
Short
Magnets
(x10)

Figure 14

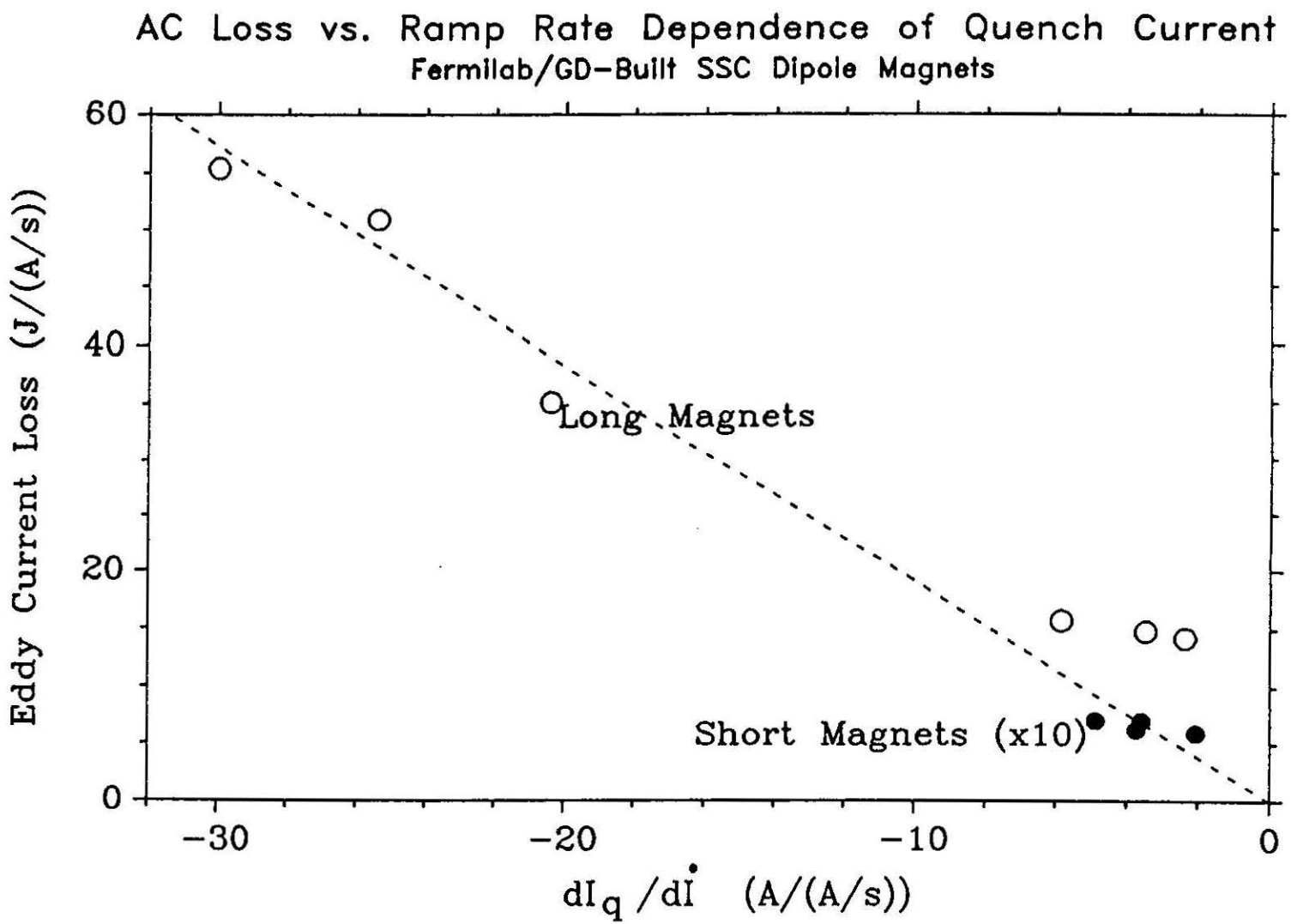
AC Loss vs. Ramp Rate Dependence of Quench Current
Fermilab/GD-Built SSC Dipole Magnets
Eddy Current Loss (J/(A/s))
60
40
20
0
Long Magnets
Short Magnets (x10)
−30
−20
−10
0
dI_q /dİ (A/(A/s))

Figure 15